Inorg. Chem. **2007**, *46*, 8372–8378

Controlled Synthesis of the $ZnWO_4$ Nanostructure and Effects on the Photocatalytic Performance

Jie Lin,[†] Jun Lin,*[,‡] and Yongfa Zhu*[,†]

Department of Chemistry, Tsinghua University, Beijing, 100084, P. R. China, and Department of Chemistry, Renmin University of China, Beijing 100872, P. R. China

Received January 26, 2007

$ZnWO_4$ photocatalysts with various morphologies were synthesized by a hydrothermal process. The effects of hydrothermal temperature and time on the crystallinity and morphology of $ZnWO_4$ catalyst were investigated. The crystallinity was enhanced with the increase of hydrothermal temperature and hydrothermal time. The formation of $ZnWO_4$ nanoparticles was controlled via kinetic process above 160 °C, and $ZnWO_4$ nanorods with a highly [100]-preferred orientation formed via the thermodynamically control process in the temperature range of 120–140 °C. The morphology and crystallinity of $ZnWO_4$ photocatalyst have a significant influence on the photocatalytic activity for aqueous Rhodamine B and gaseous formaldehyde degradation. $ZnWO_4$ nanorod catalyst showed a much higher photocatalytic activity than the nanoparticle one. The enhanced photocatalytic activity can be attributed to the anisotropic structure of nanorod.

1. Introduction

Currently, photocatalysis is considered as a promising method for solving environment problems, especially for the removal of organic contaminants with sunlight.[1] Recently, complex oxide photocatalysts, such as $NaTaO_3$,[2] Bi_2WO_6,[3] Ta_2O_5,[4] $CaBi_2O_4$,[5] and $AgInW_2O_8$,[6] have been reported to show activity for the photodegradation of organic pollutants or/and water decomposition.

Up to now, it has been confirmed that tungstate showed high photocatalytic activity on decontamination, such as Bi_2WO_6[3] and $AgInW_2O_8$.[6] $ZnWO_4$ as a kind of tungstate has received considerable attention due to its applications as an X-ray and γ-scintillator, photoanodes, and solid-state laser host, as well as for acoustic and optical fibers.[7] Our previous research showed that $ZnWO_4$ exhibited relatively high photocatalytic[8] and photoelectrocatalytic[9] activities for the mineralization of organic compounds. However, further research on the improvement of $ZnWO_4$ photocatalytic activity was still indispensable. There were several methods for the preparation of $ZnWO_4$, including solid-state reaction,[10−11] the sol−gel method,[7] the hydrothermal method,[12] and the polymerized complex method.[13] The hydrothermal method was an easy method in which to control the morphology and crystal growth orientation.[14] Although the synthesis of $ZnWO_4$ nanorods has been reported, the effect of morphology on the photocatalytic properties has not been well understood. In this work, $ZnWO_4$ photocatalysts with different morphologies were synthesized by the hydrothermal method and the relationship of morphology and photoactivity of the catalyst was revealed.

* To whom correspondent should be addressed. Phone: (+8610)-62783586 (Y.Z.); (+8610)-62516222 (J.L.). Fax: (+8610)-62787601 (Y.Z.); (+8610)-62516444 (J.L.). E-mail: zhuyf@tsinghua.edu.cn (Y.Z.); jlin@chem.ruc.edu.cn (J.L.).

† Tsinghua University.

‡ Renmin University of China.

(1) Linsebigler, A.; Lu, G.; Yates, J. T. *Chem. Rev.* **1995**, *95*, 735.
(2) He, Y.; Zhu, Y. F.; Wu, N. Z. *J. Solid. State. Chem.* **2004**, *177*, 3868.
(3) (a) Tang, J. W.; Zou, Z. G.; Ye, J. H. *Chem. Lett.* **2004**, *92*, 53. (b) Zhang, C.; Zhu, Y. F. *Chem. Mater.* **2005**, *17*, 3537. (c) Fu, H. B.; Pan, C. S.; Yao, W. Q.; Zhu, Y. F. *J. Phys. Chem. B* **2005**, *109*, 22432. (d) Fu, H. B.; Zhang, L. W.; Yao, W. Q.; Zhu, Y. F. *Appl. Catal., B* **2006**, *66*, 100.
(4) Zhu, Y. F.; Yu, F.; Man, Y.; Tian, Q. Y.; He, Y.; Wu, N. Z. *J. Solid State Chem.* **2005**, *178*, 224.
(5) Tang, J. W.; Zou, Z. G.; Ye, J. H. *Angew. Chem., Int. Ed.* **2004**, *43*, 4463.
(6) Tang, J. W.; Zou, Z. G.; Ye, J. H. *J. Phys. Chem. B* **2003**, *107*, 14265.
(7) Bonanni, M.; Spanhel, L.; Lerch, M.; Fuglein, E.; Muller, G. *Chem. Mater.* **1998**, *10*, 304.
(8) Fu, H. B.; Lin, J.; Zhang, L. W.; Zhu, Y. F. *Appl. Catal., A* **2006**, *306*, 58.
(9) Zhao, X.; Zhu, Y. F. *Environ. Sci. Technol.* **2006**, *40*, 3367.
(10) (a) Jander, W.; Wenzel, W.; Anorg, Z. *Allg. Chem.* **1941**, *240*, 67. (b) Phani, A. R.; Passacantando, M.; Lozzi, L.; Santucci, S. *J. Mater. Sci.* **2000**, *35*, 4879.
(11) Henglein, A.; Bunsenges, Ber. *Phys. Chem.* **1974**, *78*, 1078.
(12) Wen, F.-S.; Zhao, X.; Huo, H.; Chen, J.-S.; Lin, E. S.; Zhang, J.-H. *Mater. Lett.* **2002**, *55*, 152.
(13) Ryu, J. H.; Lim, C. S.; Auh, K. H. *Mater. Lett.* **2003**, *57*, 1550.
(14) Gulliver, E. A.; Garvey, J. W.; Wark, T. A.; Hampden-Smith, M. J.; Datye, A. *J. Am. Ceram. Soc.* **1991**, *24*, 1091.

10.1021/ic701036k CCC: $37.00
Published on Web 08/28/2007

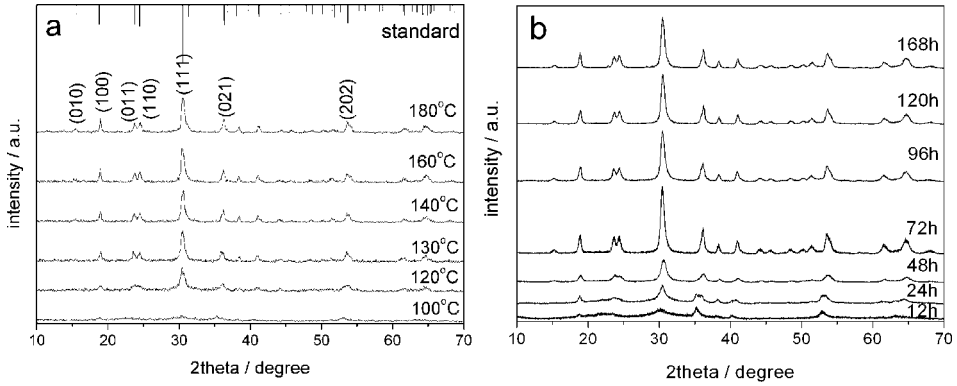

Figure 1. X-ray diffraction patterns of the samples (a) prepared at different hydrothermal temperatures for 48 h and (b) prepared at 120 °C for different hydrothermal times.

This work was devoted to revealing the formation mechanism of $ZnWO_4$ nanostructure and the effect of morphology on the photocatalytic activity. Nanostructured $ZnWO_4$ was characterized by powder X-ray diffractometry (XRD), transmission electron microscopy (TEM), the Brunauer−Emmet−Teller (BET) surface area, and ultraviolet−visible diffuse reflectance spectroscopy (UV−vis DRS) techniques. Both aqueous Rhodamine B (RhB) and gaseous formaldehyde (FAD) photodegradations were employed as probe reactions to evaluate the photocatalytic activity of $ZnWO_4$ photocatalysts under UV irradiation.

2. Experimental Section

2.1. Synthesis of Catalysts. Zinc tungstate ($ZnWO_4$) catalysts were prepared by the hydrothermal method based on the literature procedure.[15] $Na_2WO_4{\cdot}2H_2O$ (2 mmol), $Zn(NO_3)_2{\cdot}6H_2O$ (2 mmol), and cetyltrimethyl ammonium bromide (C_{16}TAB, 4 mmol) were added into a mixture of 3 mL of *n*-hexane and 30 mL of water under stirring. Then, the mixture was transferred into a Teflon-lined steel autoclave of 40 mL, and the autoclave was heated under autogenous pressure at a series of temperatures for 48 h or at 120 °C for a series of aging times. Afterward, the autoclave was cooled to room temperature gradually. The white precipitate was washed with ethanol and distilled water three times. Then, it was dried at 80 °C under vacuum for 4 h. All the samples were irradiated under UV light ($\lambda = 254$ nm, 300 $\mu W{\cdot}cm^{-2}$) for 24 h to remove possible leftover C_{16}TAB. In the system, the concentration of C_{16}TAB was 133 mM and *n*-hexane was used, so rodlike micelles formed as template according to ref 16[16] and the hydrothermal reaction occurred in rodlike micelles.

2.2. Characterization. The morphologies and microstructures of the sample were observed with a JEOL JEM 1010 transmission electron microscope operated at 120 kV. Further structural characterization was performed on FEI Tecnai F20 high-resolution field-emission transmission electron microscope (HRTEM) operated at 200 kV. XRD patterns of $ZnWO_4$ photocatalysts were recorded by a Bruker D8-advance X-ray diffractometer operated at 40 kV and 40 mA using Cu Kα radiation. UV−vis DRS was performed on a Hitachi U-3010 and $BaSO_4$ was used as a reference. Fourier transform infrared spectra (FT-IR) were recorded on a Perkin-Elmer 1600 FT-IR spectrometer with a KBr disk. BET surface area was determined by nitrogen adsorption−desorption isotherm measurements at 77 K on a Micrometrics ASAP 2010.

2.3. Measurements of Photocatalytic Activity. The photocatalytic activities were first evaluated by the decomposition of gaseous FAD under UV irradiation ($\lambda = 254$ nm). A 50-mg sample was dispersed on a uniformed glass slice (18.75 cm^2) evenly with alcohol. FAD gas (∼1400 ppm) was injected into a sealed vessel of 250 mL. After the FAD concentration reached a constant, the light irradiation started. UV light was obtained by an 11 W Hg lamp ($\lambda = 254$ nm, Institute of Electric Light Source, Beijing), and the average light intensity was 358 $\mu W{\cdot}cm^{-2}$ on the surface of $ZnWO_4$ catalysts. The concentrations of FAD were determined using a gas chromatograph (SP-502) with a flame ionization detector.

To further evaluate the photocatalytic activities of $ZnWO_4$ catalysts, the decomposition of RhB was also tested under UV irradiation ($\lambda = 254$ nm). The average UV light intensity was 125 $\mu W{\cdot}cm^{-2}$ on the solution surface, and the irradiation area was ∼40 cm^2. The aqueous suspension of RhB (200 mL, 1×10^{-5} M) containing 100 mg photocatalyst was dispersed in a vessel. Before photodegradation, an adsorption−desorption equilibrium state was established by ultrasonic and mechanical stirring for 10 min. The samples were taken from the suspension at an interval of about 20 min and centrifugated to remove the suspended particulates. Then, the concentration of RhB in solution was analyzed with a Hitachi U-3010 UV−vis spectrophotometer at 550 nm.

3. Results and Discussion

3.1. Controlled Synthesis and Formation Mechanism of $ZnWO_4$ Nanostructures. Figure 1 showed XRD patterns of $ZnWO_4$ samples prepared in different hydrothermal conditions. No diffraction peaks were found when the sample was prepared at 100 °C for 48 h. The shape of the diffraction peaks became more clean-cut and the intensities increased gradually with the increase of hydrothermal temperature from 120 to 160 °C, which indicated the crystalline structure was improved. When the hydrothermal temperature settled at 120 °C, the crystalline phase of $ZnWO_4$ appeared after hydrothermal treatment for 24 h, as shown in Figure 1b. The crystalline phase became perfect with the increase of hydrothermal time. At the top of Figure 1a, a standard XRD pattern of $ZnWO_4$ (JCPDS Card no.: 73-0554) is given. All XRD patterns could be easily identified as a pure, monoclinic tungstate structure based on a JCPDS Card (no.: 73-0554), except for the samples prepared at 120 °C for 12 h and at

(15) Xiong, Y. J.; Xie, Y.; Li, Z. Q.; Li, X. X.; Gao, S. M. *Chem. Eur. J.* **2004**, *10*, 654.
(16) Sun, Y.; Zhang, L.; Zhou, H.; Zhu, Y.; Sutter, E.; Ji, Y.; Rafailovich, M. H.; Sokolov, J. C. *Chem. Mater.* **2007**, *19*, 2065.

Table 1. Effect of Hydrothermal Conditions on the Sizes of $ZnWO_4$ Crystals

hydrothermal time (h, at 120 °C)	12	24	48	72	96	120	168
cryst size[a] (nm)	1.3	6.6	9.8	10.8	10.7	10.7	10.8
hydrothermal temp (°C, for 48 h)	100	120	130	140	160	180	
cryst size[a] (nm)	4.9	9.8	12.2	13.5	13.2	13.5	

[a] The crystal size was calculated by Scherrer equation on the basis of the (111) plane of the $ZnWO_4$ crystal.

100 °C for 48 h. The standard intensity of the (100) peak is about 3.7 times that of the (010) peak, which could be expressed as $I(100)/I(010) = 3.7$. In the XRD pattern of the nanorod sample prepared at 140 °C for 48 h, the value of $I(100)/I(010) = 10.9$. It implied the crystal had special anisotropic growth along the [100] direction, which was consistent with literature.[17] This conclusion was further confirmed by HRTEM observation below.

The crystallite size (D_{XRD}) was determined using the diffraction peak of $ZnWO_4$ (111) plane ($2\theta = 30.5°$) with Scherrer equation $D_{XRD} = 0.9\lambda/(\beta \cos \theta)$.[18] Where λ is the characteristic wavelength of the X-ray, θ is the diffraction angle, and β is the angular width in radians at an intensity equal to half of the maximum peak intensity. The results were shown in Table 1. It was clear that when the hydrothermal time increased from 12 to 72 h at 120 °C, the crystal sizes of $ZnWO_4$ crystal increased from 1.3 to 10.8 nm, and the crystal size did not increase any more when the hydrothermal time was longer than 72 h. This implied that crystal growth at 120 °C reached thermodynamics balance after the sample was hydrothermally treated for 72 h. When the hydrothermal time was constant for 48 h, the crystal size of $ZnWO_4$ increased from 4.9 to 13.5 nm with the hydrothermal temperature increasing from 100 to 140 °C, and the crystal size did not increase while the temperature further increased. The above results indicated that both hydrothermal temperature and time were the key factors of controlling crystal size.

The morphologies of $ZnWO_4$ catalysts prepared at 120 °C for various hours are shown in Figure 2. After aging for 12 h, only small particles formed (Figure 2a). The small particles are amorphous on the basis of the selected area electron diffraction (SAED) image, suggesting that no crystal nucleuses formed at 120 °C for 12 h. This result was consistent with the XRD result. After aging for 24 h (Figure 2b), the sample grew to form a nanorod structure with an obviously preferred orientation. $ZnWO_4$ nanorods with a length exceeding 100 nm were obtained after hydrothermal treatment for 72 h (Figure 2d). The length of $ZnWO_4$ nanorods was increasing with hydrothermal time until 72 h, and the diameter of $ZnWO_4$ nanorods increased slightly when the treatment time was prolonged from 24 to 72 h. After hydrothermal treatment for more than 72 h, $ZnWO_4$ nanorods did not grow in width and length any more with time,

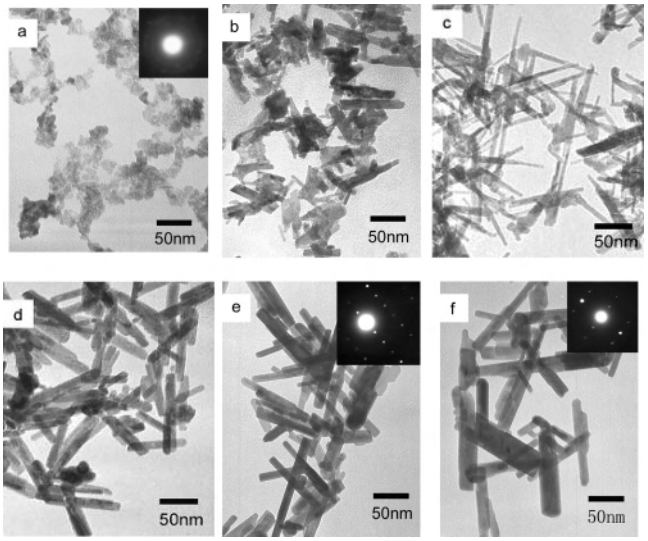

Figure 2. TEM images of the samples synthesized at 120 °C for different hydrothermal times: (a) 12, (b) 24, (c) 48, (d) 72, (e) 120, and (f) 168 h.

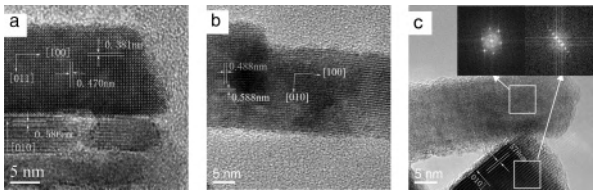

Figure 3. HRTEM images of the samples (a) prepared at 120 °C for 48 h and (b, c) prepared at 120 °C for 168 h. The inset (c) corresponds to fast two-dimensional Fourier transforms of HRTEM image at the boxed regions.

implying that thermodynamic equilibrium of growth was reached. On the basis of the above results and refs 17 and 19, it can be deduced that $ZnWO_4$ nanorod crystals originated from the epitaxial aggregation process of $ZnWO_4$ nanoparticles.

To understand the preferential orientation growth, $ZnWO_4$ samples have been further studied using high-resolution field-emission TEM (HRTEM), and the results are shown in Figure 3. HRTEM images indicated that $ZnWO_4$ nanorods existed as a single-crystal structure. It is accordance with the SAED results. The HRTEM image (Figure 3a) shows that the nanorods prepared at 120 °C for 48 h were structurally uniform with a rough edge due to defects. The lattice spacings of orthogonal lattice 0.381 and 0.470 nm corresponded to the (011) and (100) planes of the $ZnWO_4$ monoclinic cell, respectively. The lattice spacing of about 0.586 nm appeared corresponded to (010) plane at another nanorod with dislocations observed. HRTEM images of the sample prepared at 120 °C for 168 h were shown in Figure 3b and c. On the basis of the spatial arrangement of the spots in the fast Fourier transformation (FFT) pattern (left inset of Figure 3c), the set of lattice planes was derived from a single monoclinic crystal. The lattice spacings of about 0.488 and 0.588 nm in Figure 3b corresponded to the (100) and (010) planes of the $ZnWO_4$ monoclinic cell, respectively. HRTEM images and FFT patterns demonstrated that the

(17) Liu, B.; Yu, S.-H.; Li, L.; Zhang, F.; Zhang, Q.; Yoshimura, M.; Shen, P. *J. Phys. Chem. B* **2004**, *108*, 2788.
(18) Cheng, J. P.; Zhang, X. B.; Tao, X. Y.; Lu, H. M.; Luo, Z. Q.; Liu, F. *J. Phys. Chem. B* **2006**, *110*, 10348.
(19) (a) Penn, R. L.; Banfield, J. F. *Science* **1998**, *281*, 969. (b) Banfield, J. F.; Welch, S. A.; Zhang, H.; Ebert, T. T.; Penn, R. L. *Science* **2000**, *289*, 751.

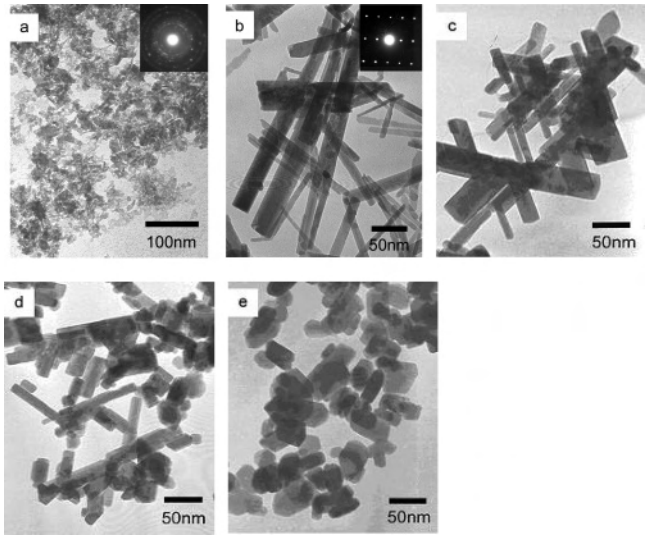

Figure 4. TEM images of the samples synthesized at different hydrothermal temperatures for 48 h: (a) 100, (b) 130, (c) 140, (d) 160, and (e) 180 °C.

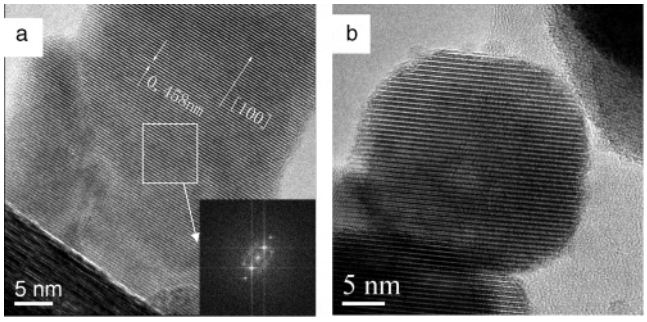

Figure 5. HRTEM images of the samples (a) prepared at 130 °C for 48 h, the inset corresponding to FFT of HRTEM image at the boxed region, and (b) prepared at 180 °C for 48 h.

nanorod grew along the [100] direction (indicated with an arrow) without dislocations. In conclusion, nanorods grew along the [100] direction at 120 °C and the dislocations of the nanorods disappeared with the increase of hydrothermal time.

The effect of hydrothermal temperature on morphologies of $ZnWO_4$ photocatalysts after hydrothermal treatment for 48 h was shown in Figure 4. The sample prepared at 100 °C for 48 h mainly showed an irregular shape with slender diffraction rings and dots (Figure 4a). After the hydrothermal temperature increased to 120 °C, uniform nanorods were obtained (Figure 2c). The nanorods grew larger and longer with the increase of hydrothermal temperature from 120 to 140 °C, and the length exceeded 100 nm at 130 and 140 °C (Figure 4b and c). The diffraction dot of the sample prepared at 130 °C (Figure 4b) indicated that the nanorod was a single crystal with perfect crystallinity. The HRTEM image of the sample prepared at 130 °C for 48 h (Figure 5a) also showed that the nanorod was structurally uniform without dislocations. A well-resolved lattice with an interplanar spacing of 0.458 nm was vertical to the preferred growth direction, which was in agreement with the distance between the (100) crystal planes. On the basis of the above results, $ZnWO_4$ nanorods prepared at 130 °C for 48 h also grew along the [100] direction.

After the hydrothermal temperature increased to 180 °C, $ZnWO_4$ photocatalysts consisted of uniform nanoparticles with regular edges (Figures 4e). The HRTEM image (Figure 5b) confirmed that the nanoparticles were well crystallized without defects and dislocations. To explore the formation mechanism of nanoparticle, the sample prepared at 130 °C for 48 h was hydrothermally re-treated at 180 °C for another 48 h. On the basis of Figure S1, the re-treated sample kept a nanorod structure, which was different from that of the nanoparticle sample prepared at 180 °C for 48 h directly (Figure 4e) and was similar to that of the nanorod sample prepared at 130 °C for 48 h (Figure 4b). This result implied that the particles did not come from the breaking of nanorods at a higher hydrothermal temperature. The formation mechanism of nanoparticles at 180 °C could be explained as quick nucleation occurred and the growth process reached balance before small particles could assemble in C_{16}TAB template. Thus, the sample prepared at 180 °C only consisted of small particles. This result also indicated that the final morphology was depended on the formation temperature of $ZnWO_4$ crystals. Once the nanorods had formed, the morphology did not change even at a higher temperature under hydrothermal condition.

On the basis of the above results, it could be concluded that the formation mechanisms of nanorods and nanoparticles were different. Nanorods formed by oriented assembling of tiny nanoparticles under low temperature,[17,19] mainly determined by the relative growth rate of various crystal planes bounding the crystal.[20] When the hydrothermal temperature was high enough, the nucleus grew up quickly and the growth of crystal reached thermodynamics equilibrium before nanoparticles assembled. Thus, the growth of crystals was governed under kinetic control and only nanoparticles formed at high hydrothermal temperatures.

3.2. Effects of Nanostructure on the Optical Properties. The influences of crystallinity and morphology on the optical properties of photocatalysts were shown in Figure 6. Only a strong broad peak appeared in the DRS curve for the $ZnWO_4$ photocatalyst with poor crystallinity (the samples prepared at 100 °C for 48 h and 120 °C for 12 h). Three peaks appeared in the range of 200−350 nm for the other samples. The peaks at 292 and 262 nm could be attributed to direct excitation in $ZnWO_4$, while the peak at 219 nm related to the electron transfer from the anion to the cation sublattice.[21] Besides, the shoulder peak around 350 nm was also observed for the samples prepared below 160 °C. On the basis of FT-IR results (Figure 7), all the samples prepared below 160 °C showed a strong IR band located at 2927, 2849, and 1470 cm^{-1} which resulted from C_{16}TAB. After the sample prepared at 120 °C for 120 h was annealed at 450 °C for 2 h in air, C_{16}TAB was removed completely, based on FT-IR results (Figure S2), and the peak around 350 nm in the DRS curve (Figure S3) also disappeared. As the annealed sample

(20) Li, W.-J.; Shi, E.-W.; Zhong, W.-Z.; Yin, Z.-W. *J. Cryst. Growth* **1999**, *203*, 186.
(21) Nagirnyi, V.; Feldbach, E.; Jönsson, L.; Kirm, M.; Kotlov, A.; Lushchik, A.; Nefedov, V. A.; Zadneprovski, B. I. *Nucl. Instrum. Methods A* **2002**, *486*, 395.

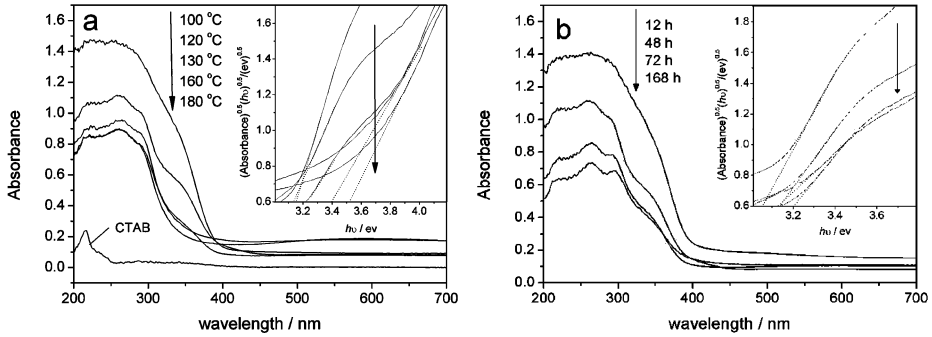

Figure 6. Diffuse reflectance absorption spectra of $ZnWO_4$ samples (a) prepared at different hydrothermal temperatures for 48 h and (b) prepared at 120 °C for different hydrothermal times. The inset was the $(\text{absorbance})^{0.5}(h\nu)^{0.5}$ versus photon energy plots.

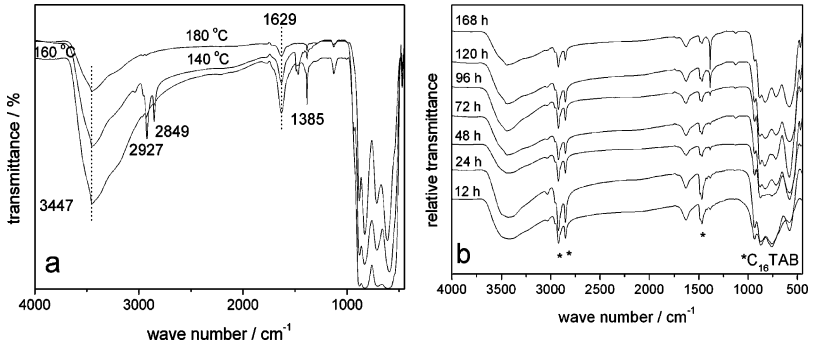

Figure 7. Fourier transform infrared spectra of nanostructured $ZnWO_4$ (a) samples obtained in temperature range of 140−180 °C for 48 h and (b) samples obtained at 120 °C for various hydrothermal times.

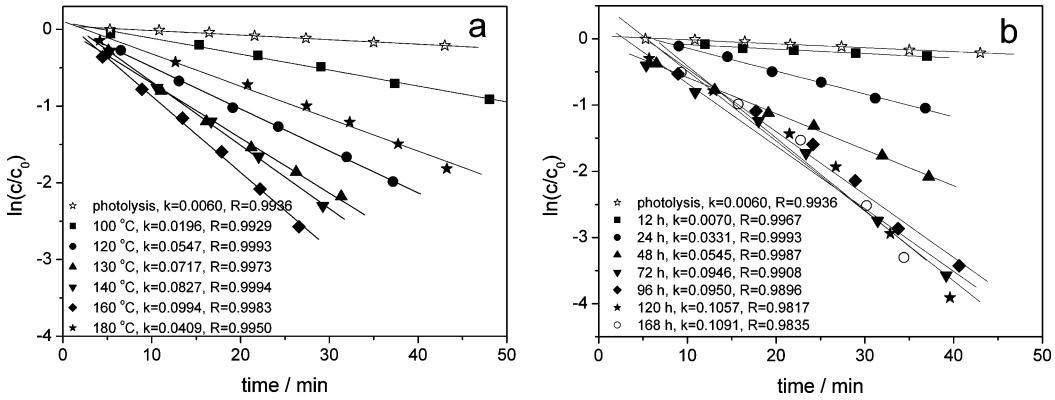

Figure 8. Photocatalytic degradations of FAD under UV irradiation ($\lambda = 254$ nm) by the samples (a) prepared at different hydrothermal temperatures for 48 h and (b) prepared at 120 °C for different hydrothermal times. Photocatalyst: 0.05 g; FAD, 1400 ppm in air.

kept a nanorod structure (Figure S4), it indicated that the peak at 350 nm came from the leftover C_{16}TAB.

The band gap energies estimated from the $(\text{absorbance})^{0.5}$-$(h\nu)^{0.5}$ versus photon energy plots (inset of Figure 6a) were 3.15, 3.13, 3.21, 3.39, and 3.52 eV for $ZnWO_4$ samples prepared at 100, 120, 130, 160, and 180 °C for 48 h, and the band gap energies of the samples prepared at 120 °C for 12, 48, 72, and 168 h (inset of Figure 6b) were 3.05, 3.13, 3.20, and 3.13 eV, respectively. The band gap energies of $ZnWO_4$ photocatalysts were coincident with the literature.[8] The band gap of the sample was enlarged observably with the increase of hydrothermal temperature, but the influence of hydrothermal time on the band gap was slight. It was found that the band gap of nanorods was narrower than that of nanoparticles. The leftover C_{16}TAB in nanorod partly influenced the band gap of $ZnWO_4$ prepared below 160 °C.

3.3. Effects of Nanostructure on the Photocatalytic Activities. Gaseous FAD degradation was chosen as a model reaction to evaluate photocatalytic activities of $ZnWO_4$ samples. All the samples were evenly dispersed on a uniformed glass slice (18.75 cm^2) and had same surface area exposed to UV light. Because all the samples were the same material, the light scattering effect was similar and could be ignored. Comparing the direct photolysis data in Figure 8, all the samples, except for that prepared at 120 °C for 12 h, had obvious photocatalytic activities on degradation of FAD. The photocatalytic activities of the samples prepared at 120−160 °C for FAD degradation increased with hydrothermal temperature. When the hydrothermal temperature was lower than 120 °C, the sample showed less photocatalytic activity due to its poor crystallinity. According to the BET results (shown in Table 2), the sample prepared at 120 °C for 48 h

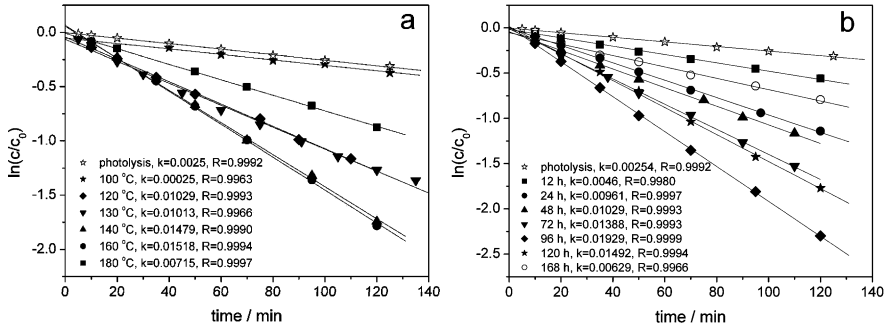

Figure 9. Photocatalytic degradations of RhB by the as-prepared samples: (a) prepared at different hydrothermal temperatures for 48 h and (b) prepared at 120 °C for different hydrothermal times. Catalyst loading, 0.5 g/L; RhB, 1×10^{-5} M; $\lambda = 254$ nm; pH of the working solutions were not controlled.

Table 2. BET Surface Area of $ZnWO_4$ Samples Prepared at Different Hydrothermal Temperatures for 48 h

hydrothermal temp (°C)	100	120	130	180
surface area (m^2/g)	23.8	30.1	23.1	20.4

had a larger surface area than that prepared at 130 °C, while the latter one exhibited a better crystallinity without dislocations and defects, based on the XRD results and HRTEM images. The sample prepared at 130 °C for 48 h showed a higher photocatalytic activity, revealing that the crystallinity played a more important role in the photoactivity than the surface area did. The same conclusion was also obtained for the time series samples. With an improvement in the crystallinity, the photocatalytic activities of the samples increased.

There were two peaks at 3447 and 1629 cm^{-1} in the IR spectra of all samples in Figure 7, implying that the basic hydroxyl groups existed in all $ZnWO_4$ samples.[22] These results clearly indicated that the surface of all samples was hydroxylated. Another IR peak at 1385 cm^{-1} resulted from OH^- absorption of hydrogen-related defects.[23] As shown in Figure 7b, the intensity of IR peak at 1385 cm^{-1} became stronger with the increase of hydrothermal time from 72 to 168 h. It could be ascribed to the increase of defects in crystals under hydrothermal condition,[24] but the photocatalytic activity of FAD degradation varied slightly in the range of 72−168 h, which suggested that hydrogen-related defects played a small role in the photodegradation of FAD. Thus, the hydrogen-related defect was not the main factor to the high photocatalytic activity of nanorod sample.

Although the crystallinities of $ZnWO_4$ photocatalysts prepared in the temperature range from 130 to 180 °C for 48 h were similar, their photocatalytic activities were also different, implying that the morphology of $ZnWO_4$ also had a great influence on photocatalytic activity. On the basis of DRS results, the band gap of the nanorod samples was narrower than that of the nanoparticle samples. The influence of band gap on photocatalytic activity can be ignored due to enough excitation energy of 254 nm. On the basis of former research, the photocatalytic ability of $ZnWO_4$ was attributed to the transition of the electrons from the valence band (purely composed of the O 2p orbital) to the conduction band (the hybrid orbitals of W 5d and O 2p) in the catalyst.[8] According to HRTEM results (Figures 3 and 5), nanorods had more planes along the [100] direction and nanoparticles had no obvious crystal orientation. The $ZnWO_4$ (100) plane mainly consisted of Zn and O atoms, so the (100) plane may be less active for photocatalytic activity than the ones along the [100] direction. In other words, the planes containing W and O atoms along the [100] direction were more active and the enhanced photocatalytic activity of nanorods was attributed to the more active planes along the [100] direction.

In conclusion, the crystallinity and morphology of $ZnWO_4$ photocatalyst were the main factors for FAD photodegradation, while the hydrogen-related defect was less important. The planes along the [100] direction, such as the (010) and (011) planes, would be more active for photodegradation.

The photodegradation of RhB was also used to evaluate photocatalytic activities of $ZnWO_4$, and the results are shown in Figure 9. All the samples, except for the one prepared at 100 °C for 48 h, exhibited photocatalytic activities for RhB degradation. The photocatalytic activities of the samples prepared for 24 h increased with the increase of hydrothermal temperature from 120 to 140 °C, and decreased from 160 to 180 °C. The sample prepared at 160 °C had a similar photocatalytic activity to the one prepared at 140 °C. When the hydrothermal temperature was kept at 120 °C, the photocatalytic activities of the samples increased with the increase of hydrothermal time from 12 to 96 h and decreased when the hydrothermal time was more than 96 h. Both hydrothermal temperature and time had significant effects on the photocatalytic activities of $ZnWO_4$ photocatalysts. This result is similar to the results of FAD degradation; crystallinity and morphology were the main factors to influence the photocatalytic activities of RhB degradation. In general, defects in photocatalysts were recombination centers of photoinduced electrons and holes, which would result in the decrease of photocatalytic activity.[24] Thus, the photocatalytic activity decrease of the samples prepared at 160 °C for 48 h can be attributed to the existence of OH^- defects, comparing with the degradation of FAD. When the reaction temperature was kept at 120 °C, the photocatalytic activity decrease of the samples prepared for more than 96 h can also be attributed to the existence of OH^- defects in the photocatalyst. In a word, except for crystallinity and

(22) Gotic, M.; Ivanda, M.; Popovic, S.; Music, S. *Mater. Sci. Eng., B* **2000**, *B77*, 193.
(23) Li, Z. S.; Yu, T.; Zou, Z. G.; Ye, J. H. *Appl. Phys. Lett.* **2006**, *88*, 071917.
(24) Xu, T.-G.; Zhang, C.; Shao, X.; Wu, K.; Zhu, Y.-F. *Adv. Funct. Mater.* **2006**, *16*, 1599.

morphology, hydrogen-related defects also played an important role on the photocatalytic activity in aqueous system.

4. Conclusions

$ZnWO_4$ nanoparticles and nanorods were successfully synthesized by the hydrothermal process. $ZnWO_4$ nanoparticles formed above 160 °C via kinetic control and $ZnWO_4$ nanorods with a highly [100]-preferred orientation were obtained in a range of 120−140 °C via thermodynamic control. The photocatalytic activity of nanorods is much higher than that of nanoparticles. The [100]-preferred orientation growth of the nanorods and perfect crystallinity can enhance the photocatalytic activity of $ZnWO_4$ catalyst, and the hydrogen-related defects have more influences on the aqueous photodegradation system than on the gaseous one.

Acknowledgment. This work was partly supported by Chinese National Science Foundation (20433010, 20571047).

Supporting Information Available: Additional figures. This material is available free of charge via the Internet at http://pubs.acs.org.

IC701036K